The Journal of Chemical Physics

Alignment and propulsion of squirmer pusher–puller dumbbells

Cite as: J. Chem. Phys. **156**, 194901 (2022); https://doi.org/10.1063/5.0091067
Submitted: 11 March 2022 • Accepted: 27 April 2022 • Accepted Manuscript Online: 28 April 2022 • Published Online: 16 May 2022

Judit Clopés, Gerhard Gompper and Roland G. Winkler

The Journal of Chemical Physics ARTICLE scitation.org/journal/jcp

Alignment and propulsion of squirmer pusher–puller dumbbells

Cite as: J. Chem. Phys. 156, 194901 (2022); doi: 10.1063/5.0091067
Submitted: 11 March 2022 • Accepted: 27 April 2022 •
Published Online: 16 May 2022

Judit Clopés, Gerhard Gompper,[a] and Roland G. Winkler[a]

AFFILIATIONS

Theoretical Physics of Living Matter, Institute of Biological Information Processing and Institute for Advanced Simulation, Forschungszentrum Jülich, 52425 Jülich, Germany

[a]Authors to whom correspondence should be addressed: g.gompper@fz-juelich.de and r.winkler@fz-juelich.de

ABSTRACT

The properties of microswimmer dumbbells composed of pusher–puller pairs are investigated by mesoscale hydrodynamic simulations employing the multiparticle collision dynamics approach for the fluid. An individual microswimmer is represented by a squirmer, and various active-stress combinations in a dumbbell are considered. The squirmers are connected by a bond, which does not impose any geometrical restriction on the individual rotational motion. Our simulations reveal a strong influence of the squirmers' flow fields on the orientation of their propulsion directions, their fluctuations, and the swimming behavior of a dumbbell. The properties of pusher–puller pairs with an equal magnitude of the active stresses depend only weakly on the stress magnitude. This is similar to dumbbells of microswimmers without hydrodynamic interactions. However, for non-equal stress magnitudes, the active stress implies strong orientational correlations of the swimmers' propulsion directions with respect to each other, as well as the bond vector. The orientational coupling is most pronounced for pairs with large differences in the active-stress magnitude. The alignment of the squirmers' propulsion directions with respect to each other is preferentially orthogonal in dumbbells with a strong pusher and weak puller, and antiparallel in the opposite case when the puller dominates. These strong correlations affect the active motion of dumbbells, which is faster for strong pushers and slower for strong pullers.

I. INTRODUCTION

Hydrodynamics plays a fundamental role in the motion of micro-organisms, in general, and microswimmers, in particular, as the vast majority of them are embedded in a liquid environment. A wide spectrum of micro-organisms generates distinctive flow fields for specific vital purposes, such as motility, feeding, and mechanosensing.[1,2] Other factors, such as geometric constraints, interfaces, or the presence of nearby other microswimmers, also affect their behaviors.[3–8] The self-generated flow field of a microswimmer can be rather complex[9–11] and depends distinctively on its actual actuation mechanism. Microswimmers with the propulsion at the front are classified as pullers, e.g., *Chlamydomonas reinhardtii*, and those with propulsion at the rear as pushers, e.g., *Escherichia coli*.[12–14] Their hydrodynamic far field is well approximated by a force dipole due to their force- and torque-free nature in absence of external forces, however, with opposite signs.[12–14] This distinction gives rise to unique characteristic behaviors; for instance, pushers align parallel to solid surfaces, whereas pullers align along the normal direction.[13–16]

The coexistence of pushers and pullers in nature is the rule rather than the exception, e.g., mixtures of algae and bacteria in the ocean. Such systems exhibit nonequilibrium fluctuations in the fluid flow due to their opposite swimming patterns, and a change in the mean swimming speed of the two populations.[17] Theoretical considerations predict that, in 1:1 mixtures of pushers and pullers, two-point hydrodynamic correlations are equal to those of a suspension of noninteracting swimmers.[18] In contrast, asymmetric concentrations yield a plethora of different mesoscale motion patterns and a strong influence of the pusher–puller composition on the ordered collective motion.[19] These studies indicate a route to control and tune the orientational order and the collective motion in active microswimmer suspensions by combining antagonistic swimmer types.

The design of a synthetic self-propelling micromachine (microbot) poses major challenges. The development of suitable concepts for autonomous and steerable motion constitutes a major advancement in the strive to create microbots.[14,20–28] Even more, smart synthetic micromachines need to be able to adopt and respond autonomously to their environment in order to perform a predefined task, such as targeted drug delivery.[27] A promising route in this endeavor is to build a microbot from different components with specific functionality, such as controlled propulsion or sensing. In this context, the understanding of the nature of pusher–puller interactions in stable assemblies could be fundamental for the design of optimized synthetic micromachines or even bio-hybrid microswimmer-based artificial devices.[21,22,28,29]

To shed light onto the emergent swimming properties of pusher–puller assemblies, we study the characteristics of dumbbells comprising a pusher and a puller squirmer, which are connected by a bond, maintaining a nearly constant spatial separation. Such dumbbells constitute a minimal model suitable for studying the fundamental interactions between antagonistic microswimmers. The squirmer model itself was initially intended to describe multi-ciliated micro-organisms, such as *Paramecia*,[30,31] but has been extended to encompass diverse self-propelled entities due to its simplicity and generic character.[5,32,33] In addition, several other dumbbell-type models for microswimmers, not composed of squirmers, have been proposed.[34–36]

Previous theoretical and simulation studies[23,37] on the influence of the microswimmer flow fluid on the properties of squirmer dumbbells composed of pairs of either pushers or pullers reveal a strong influence of thermal fluctuations and orientational degrees of freedom on their swimming ability.[37] In particular, a far-field consideration predicts that no stable forward swimming can be achieved for freely rotating, torque-free squirmer dumbbells, whereas a restricted rotational motion of the individual squirmers by (rigid) bonds implies torques and stable swimming motion.[23] Thermal fluctuations fundamentally alter the swimming properties of such dumbbells.[37] The fluctuations imply a rotational diffusive motion of the individual squirmers and lead to swimming. Despite the fluctuations, the squirmers' propulsion directions assume preferred activity-dependent average directions in the stationary state, which strongly affects their mean-square displacement; the latter is the largest for weak pushers and the smallest for strong pullers. For puller–pusher pairs, theoretical studies predict stable swimming when the trailing squirmer is a strong pusher with an enhanced swimming speed compared to that of the individual squirmers.[23]

In this study, we analyze the properties of freely rotating pusher–puller squirmer pairs linked by a finite-length bond in a three-dimensional unbounded fluid. The fluid is described by the multiparticle collision (MPC) dynamics method, a particle-based mesoscale simulation approach including thermal fluctuations.[38,39] MPC has successfully been applied in a broad range of soft active matter studies, especially involving squirmers.[5,16,34,37,40–45]

Our study reveals a strong influence of the squirmers' flow fields on their relative orientation, their orientation with respect to the bond vector, and the dumbbells dynamics. In terms of the active-stress dependence, we observe weak effects as long as the magnitude of the active stresses of the pusher and puller are equal. In contrast, strong effects appear for pairs with large relative differences in the active-stress magnitude. The alignment of the propulsion directions is found to be preferentially orthogonal with respect to each other in dumbbells with a large pusher and a small puller active stress, and antiparallel in the opposite case when the puller dominates. These strong correlations imply a drastically different dynamics, which is faster for strong pushers and slower for strong pullers.

This article is structured as follows: In Sec. II, the model is described and the simulation approach is presented. The orientational dynamics is studied in Sec. III, the properties of the bond in Sec. IV, and the stationary-state orientation of the propulsion directions with respect to each other and the bond vector in Sec. V. In Sec. VI, results for the squirmer dynamics are presented. Finally, Sec. VII summarizes our findings and presents the conclusions.

II. MODEL

A. Dumbbell model

The dumbbell is composed of two microswimmers, which are linked by the harmonic potential,

$$U = \frac{\kappa}{2}(|\boldsymbol{R}| - l)^2 \tag{1}$$

of finite bond length l. Here, $\boldsymbol{R} = \boldsymbol{r}_2 - \boldsymbol{r}_1$ is the bond vector between the microswimmers centers of mass located at $\boldsymbol{r}_1$ and $\boldsymbol{r}_2$, and κ is the spring constant (cf. Fig. 1).

The microswimmers are modeled as squirmers—rigid spherical colloidal particles of diameter σ, mass M, and the prescribed axisymmetric tangential slip velocity

$$\boldsymbol{u}_k^{sq} = \frac{3}{2}v_0\left[1 + \beta_k(\boldsymbol{e}_k \cdot \boldsymbol{e}_k^s)\right]\left[(\boldsymbol{e}_k \cdot \boldsymbol{e}_k^s)\boldsymbol{e}_k^s - \boldsymbol{e}_k\right] \tag{2}$$

on their surfaces.[5,30,31,33,37] Here, $\boldsymbol{e}_k$ is the unit vector in the direction of the propulsion of squirmer k ($k \in \{1,2\}$) and $\boldsymbol{e}_k^s$ the unit vector from a squirmer's center to its surface. The active stress is characterized by β_k and determines the nature of the propulsion—for pullers $\beta_k > 0$, for pushers $\beta_k < 0$, and for neutral squirmers $\beta_k = 0$. Without loss of generality, we consider the squirmer $k = 1$ as puller and $k = 2$ as pusher. Their propulsion directions are affected by thermal fluctuations and their flow fields. We characterize the squirmer activity by the Péclet number *Pe* defined as[14,46]

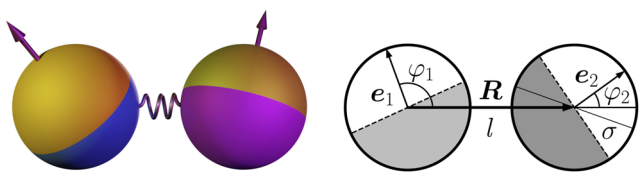

FIG. 1. Sketch of the squirmer dumbbell system. The squirmers of diameter σ are connected by the bond vector $\boldsymbol{R}$ of rest length l and are propelled in the directions $\boldsymbol{e}_1$ and $\boldsymbol{e}_2$. The shading indicates the different propulsion mechanisms, where the first squirmer ($k = 1$) is a puller and the second squirmer ($k = 2$) is a pusher.

$$Pe = \frac{v_0}{D_R^0 \sigma}, \tag{3}$$

where v_0 and D_R^0 are the swim velocity and the rotational diffusion coefficient of a single squirmer in a three-dimensional dilute solution, respectively.

B. Fluid model: Multiparticle collision dynamics (MPC)

MPC describes the fluid as N point particles of mass m. The particle positions $\boldsymbol{r}_i$ and velocities $\boldsymbol{v}_i$ $(i = 1, \ldots, N)$ are updated in two alternating steps—streaming and collision.[37–39] During the streaming step, the MPC particles move ballistically for a collision time h, and their positions are updated as

$$\boldsymbol{r}_i(t+h) = \boldsymbol{r}_i(t) + h\boldsymbol{v}_i(t). \tag{4}$$

The interactions between fluid particles take place in the collision step. Here, the particles are sorted into the cells of a cubic lattice of mesh size a that defines the local interaction environment. The velocities of the fluid particles after the collision, $\boldsymbol{v}_i(t+h)$, are given by[47,48]

$$\boldsymbol{v}_i(t+h) = \boldsymbol{v}_{cm}(t) + \mathbf{R}(\alpha)\boldsymbol{v}_{i,\mathrm{cm}}(t) - \boldsymbol{r}_{i,\mathrm{cm}} \times \left[m\mathbf{I}^{-1} \sum_{j \in \mathrm{cell}} \boldsymbol{r}_{j,\mathrm{cm}} \times \left(\boldsymbol{r}_{j,\mathrm{cm}} - \mathbf{R}(\alpha)\boldsymbol{v}_{j,\mathrm{cm}} \right) \right] \tag{5}$$

within the stochastic rotation dynamics (SRD) variant of MPC, with local linear and angular momentum conservation (MPC-SRD+a).[5,47] Here, $\mathbf{R}(\alpha)$ is the rotation matrix for the rotation of the relative velocities $\boldsymbol{v}_{i,\mathrm{cm}} = \boldsymbol{v}_i - \boldsymbol{v}_{cm}$ with respect to the cell's center-of-mass velocity $\boldsymbol{v}_{cm}$, where the ith particle belongs to. The rotation is performed around a randomly oriented axis by a fixed angle α.[49] The axis orientation is chosen independently for every cell and for every collision step. $\mathbf{I}$ is the moment-of-inertia tensor of the particles in the cell's center-of-mass reference frame, and $\boldsymbol{r}_{i,\mathrm{cm}}$ is the position of the ith particle with respect to the center-of-mass position $\boldsymbol{r}_{cm}$ of the particles in the cell. The discretization of space in a lattice breaks the Galilean invariance, which is restored by a random shift of the collision lattice at each collision step.[50] The cell level Maxwell–Boltzmann-scaling (MBS) canonical thermostat is applied to maintain a constant temperature.[49] The MPC algorithm is highly parallel, which we exploit by employ a graphics processor unit (GPU)-based version for a high performance gain.[51]

C. Coupling squirmers and MPC fluid

The spherical squirmers are neutrally buoyant and are characterized by their center-of-mass position $\boldsymbol{r}_k$, propulsion direction $\boldsymbol{e}_k$, translational velocity $\boldsymbol{v}_k$, and angular momentum $\boldsymbol{L}_k$. Their dynamics proceeds in two steps in order to account for the interactions with the MPC particles.[5,37,45] In brief (details are described in Refs. 5 and 16):

1. Streaming step

During the MPC streaming step, the squirmers move according to their rigid-body dynamics, where the rotational dynamics is described by quaternions.[5,52] Interactions with overlapping fluid particles result in changes in the colloids' linear and angular momenta, especially the squirming velocity $\boldsymbol{u}_k^{sq}$ is transferred to the MPC fluid.

2. Collision step

To implement no-slip boundary conditions, phantom particles of the same mass and density as the MPC fluid are uniformly distributed inside a squirmer, and Maxwellian-distributed thermal velocities are assigned to them in addition to the translational and rotational velocities of the colloid itself.[5,53] The phantom particles are taken into account in the collision step [Eq. (5)] in cells overlapping with the colloid. The appearing linear and angular momenta changes of phantom particles are transferred to the colloidal particle.[5]

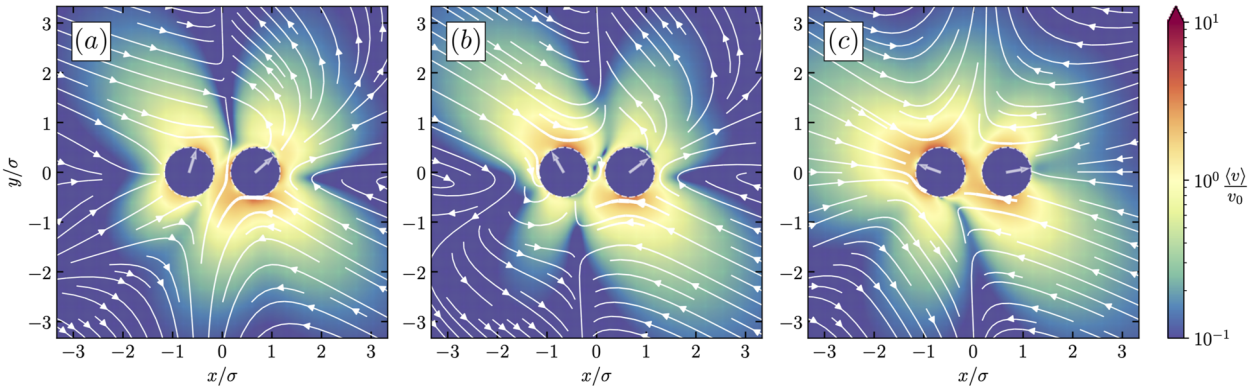

FIG. 2. Squirmer dumbbell flow fields in the laboratory reference frame for different active stresses, (a) $(\beta_1, \beta_2) = (1, -5)$, (b) $(3, -3)$, and (c) $(5, -1)$. Squirmer 1 is located at $x/\sigma = -1$ and squirmer 2 at $x/\sigma = 1$. The orientations of the squirmers' propulsion directions are indicated by arrows. The flow fields have been obtained by a superposition of the exact flow fields of the individual squirmers[5,54] and the Stokeslets emerging from the bond force, where the propulsion directions and the bond vector are assumed to be in the same plane. The Stokeslets by the bond force give rise to a force dipole (see the supplementary material, movies M1–M3).

D. Parameters

The squirmer diameter is $\sigma = 6a$ and its mass $M = 4m\pi(\sigma/2)^3\langle N_c\rangle/3$, where $\langle N_c\rangle = 10a^{-3}$ is the average number of MPC fluid particles per collision cell. The bond length is $l = 8a$ and the spring constant $k = 5000k_BT/(ma^2)$, with the Boltzmann constant k_B and the temperature T. The ratio $l/\sigma = 4/3$ is small enough to ensure pronounced hydrodynamic interactions between the two squirmers.[37] The rigid-body equations of motion are integrated by using the time step $\Delta t = 2\times10^{-3}\sqrt{ma^2/(k_BT)}$. For the MPC fluid, the collision time is $h = 0.05\sqrt{ma^2/(k_BT)}$ and the rotation angle $\alpha = 130°$. These parameters yield the MPC fluid viscosity $\eta = 7.2\sqrt{mk_BT/a^4}$[48] and the rotational diffusion coefficient $D_R^0 = 2.2\times10^{-4}\sqrt{k_BT/(ma^2)}$ for an individual passive colloid or squirmer. Three-dimensional periodic boundary conditions are applied, with a cubic simulation box of side length $L = 40a$. Results are obtained by averaging over at least five independent realizations for $Pe \lesssim 30$ and three for $Pe = 60$ due to the weaker effects by thermal fluctuations in the latter case. In each realization, 10^7 MPC steps have been performed, which correspond to a displacement of 10^3a of a single squirmer.

The considered range of swim velocities $v_0/\sqrt{k_BT/m} = (4/3–8)\times10^{-2}$, corresponding to Péclet numbers $Pe = 10, -60$, ensures small Reynolds numbers $\mathrm{Re} = v_0\sigma/\nu = 0.12–0.72 < 1$, where $\nu = \eta/(m\langle N_c\rangle/a^3)$ is the kinematic viscosity. These Reynolds numbers are an upper limit obtained for individual squirmers, which typically move faster than a dumbbell.

III. ORIENTATIONAL DYNAMICS

A. Orientational dynamics of individual squirmer in a dumbbell

The swimming direction of a squirmer in dilute solution varies due to thermal fluctuations, and the autocorrelation function for the propulsion direction exhibits the exponential decay,

$$\langle \boldsymbol{e}_k(t)\cdot\boldsymbol{e}_k(0)\rangle = e^{-2D_R^0 t}, \tag{6}$$

similar to that of an active Brownian particle (ABP).[5,14,37] Once assembled in a dumbbell, the flow fields (cf. Fig. 2) of the two squirmers interfere with each other and affect their rotational dynamics. Moreover, the bond force implies Stokeslets, which additionally influence the squirmers' dynamical properties. Figure 2 illustrates the emerging flow fields and their differences for various propulsion directions and combinations of active stresses. The flow field of an individual squirmer is obtained by the full analytical solution of the corresponding Stokes equation with the boundary condition of Eq. (2).[5] The flow fields of the two squirmers, together with those of the Stokeslets of the bond force, are then superimposed. As a consequence, the boundary condition at the squirmer surface is not exactly fulfilled; yet, the various figures qualitatively capture the complexity of the flow fields.

Figure 3(a) displays the autocorrelation functions of the squirmers' swimming direction for pusher–puller pairs with various combinations of the active stresses β_1 and β_2. The autocorrelation functions, identical for the two squirmers, deviate from a single-exponential decay to different degrees. The decay rate depends on the strength of the active stress, with a larger effective rotational diffusion coefficient compared to an individual ABP for most combinations, except for the combination $(\beta_1,\beta_2) = (5,-1)$. The latter is a consequence of the nearly antiparallel average stationary-state alignment of the two propulsion directions (Sec. V A). Two effects contribute to the decay of the autocorrelation function—the random orientational dynamics of an individual squirmer and the overall rotational diffusion of the dumbbell mainly driven by the active squirmer motion (cf. Sec. III B and the supplementary material, movies M1–M3). Thereby, the respective contribution depends on the active stresses β_k.

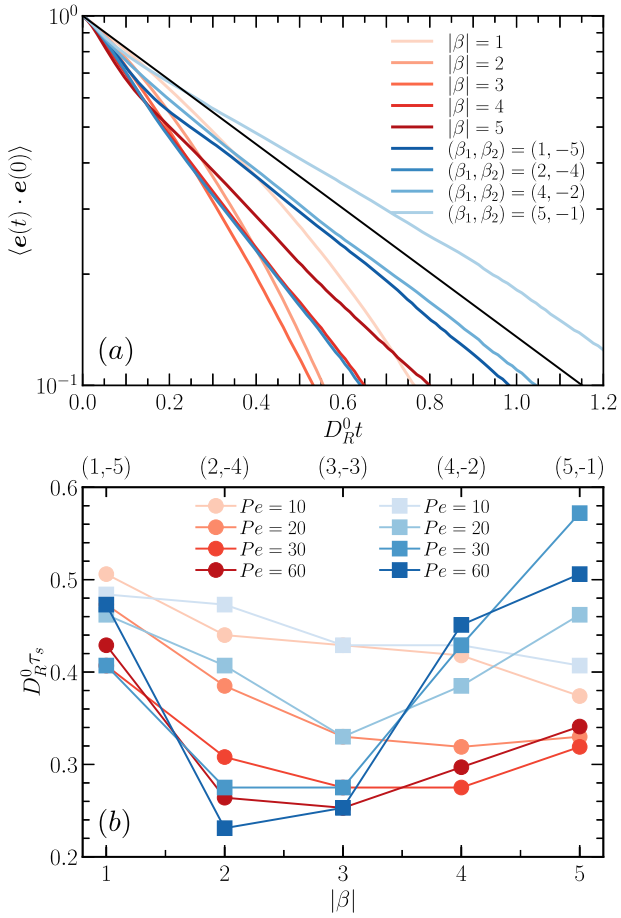

FIG. 3. (a) Autocorrelation function of a squirmer's propulsion direction in a dumbbell as a function of the scaled time $D_R^0 t$ at $Pe = 30$ and various active-stress pairs $\beta_1 = |\beta_2|$ as well as $\beta_1 \neq |\beta_2|$ as displayed in the legend. The autocorrelation functions of the two squirmers are equal, hence, $\langle \mathbf{e}(t)\cdot\mathbf{e}(0)\rangle = (\langle \mathbf{e}_1(t)\cdot\mathbf{e}_1(0)\rangle + \langle \mathbf{e}_2(t)\cdot\mathbf{e}_2(0)\rangle)/2$. D_R^0 is the rotational diffusion coefficient of an individual squirmer in an unbounded fluid. The black solid line indicates the orientation autocorrelation function of an active Brownian particle [Eq. (6)]. (b) Normalized characteristic decay times $D_R^0\tau_s$ of the propulsion direction autocorrelation function for various active-stress pairs (β_1,β_2) and Péclet numbers (see legend). The blue symbols indicate results for various pairs (β_1,β_2) (top-axis). The red symbols are for pairs $\beta_1 = |\beta_2|$ (bottom axis). The value for an ABP is $D_R^0\tau_s = 1/2$.

To quantify the decay of the autocorrelation function, we define the characteristic time τ_s as the time, where the correlation function has decreased to $1/e$ of its initial value at $t = 0$, i.e., $\langle \boldsymbol{e}_k(\tau_s) \cdot \boldsymbol{e}_k(0)\rangle = 1/e$. As Fig. 3 indicates, τ_s depend only weakly on $|\beta_k|$ for pairs with $\beta_1 = |\beta_2|$, specifically for $|\beta_k| > 1$, with the largest τ_s values for $|\beta_k| = 1$. Large variations are obtained for dumbbells with $\beta_1 \neq |\beta_2|$, specifically for larger Pe. At $Pe \gtrsim 30$, Fig. 3(b) shows a strong drop of τ_s for the change from $(\beta_1, \beta_2) = (1, -5)$ to $(2, -4)$, followed by a strong τ_s increase with increasing strength of the active stress of the puller and decreasing stress magnitude of the puller.

B. Bond vector autocorrelation function

The bond vector autocorrelation function of a dumbbell with two ABP monomers (no hydrodynamic interactions) can be calculated analytical as

$$\langle \boldsymbol{R}(t) \cdot \boldsymbol{R}(0)\rangle = l^2 e^{-t/\tau_l} + \frac{2v_0^2\tau_l^2}{1-(\gamma_R\tau_l)^2}\left(e^{\gamma_R t} - e^{-t/\tau_l}\right), \tag{7}$$

where $\gamma_R = 2D_R^0$ and the relaxation time τ_l depends on the activity.[46] In the asymptotic limit of large activity, $Pe \to \infty$, the correlation function becomes $\langle \boldsymbol{R}(t) \cdot \boldsymbol{R}(0)\rangle = l^2 \exp(-2D_R^0 t)$, as for the propulsion direction $\boldsymbol{e}$ of a single ABP.[37,46]

The bond vector autocorrelation functions of dumbbells exhibit a qualitatively similar behavior as those of the propulsion directions, with an approximate exponential decay, reflecting the tight coupling between squirmer propulsion and the active dumbbell rotational diffusion. The corresponding characteristic relaxation times τ_b are presented in Fig. 4. For $\beta_1 = |\beta_2|$, τ_b essentially decrease with increasing $|\beta_k|$. Except for $\beta_1 = 1$ and 2 for $Pe = 10$, all τ_b values are smaller than the value of an ABP dumbbell $D_R^0\tau_b = 1/2$. In contrast, for $\beta_1 \neq |\beta_2|$, τ_b increase with increasing β_1 and decreasing $|\beta_2|$. An

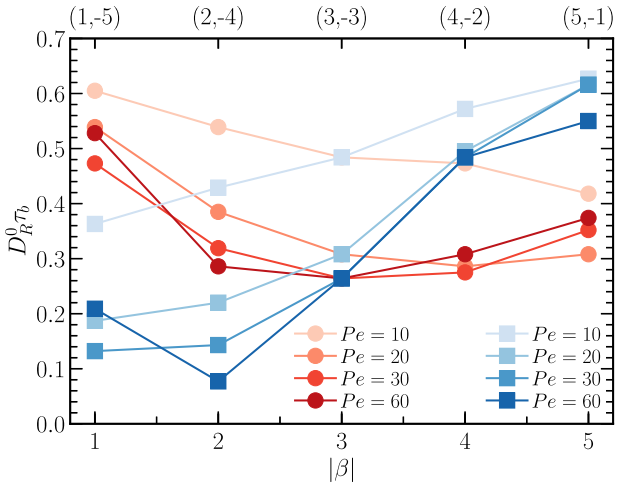

FIG. 4. Characteristic decay times $D_R^0\tau_b$ of the bond vector autocorrelation function for various active-stress pairs (β_1, β_2) and Péclet numbers (see legend). The top-axis scale indicates various pairs (β_1, β_2) for the blue symbols. The red symbols are for pairs $\beta_1 = |\beta_2|$ (bottom axis).

increasing Pe amplifies the difference between the minimum and the maximum values of τ_b for the considered range of Pe. In general, the combination of $\beta_1 \neq |\beta_2|$ and small β_1 exhibits a slow rotational dynamics, and the relaxation times are even smaller than for an ABP dumbbell. In contrast, the combination of a strong puller and weak pusher accelerates the relaxation, as for the correlation function of the propulsion direction.

This active-stress dependence is very different from that of squirmer dumbbell pairs with equal active stresses $(\beta_1 = \beta_2)$, where long relaxation times in the range of $-1 < \beta < 2$ have been observed.[37] More importantly, those correlation functions assume negative values for $\beta \leq -3$, indicating a rotational motion of the whole dumbbell, a motility pattern absent in the considered pusher–puller dumbbells.

IV. BOND FORCE

The bond exerts a force on the squirmers by their activity and thermal fluctuations. The force on squirmer k follows from the harmonic potential (1) as $\boldsymbol{F}_k = -(-1)^k F_b \boldsymbol{R}/|\boldsymbol{R}|$, with $F_b = \kappa(|\boldsymbol{R}| - l)$.

As displayed in Fig. 5, the average bond force $\langle F_b\rangle$ is positive for all combinations of β_1, β_2, and Péclet numbers, i.e., the active forces pull on the bond. This preference is related to the instability of configurations, where the propulsion directions point toward each other, i.e., for $\pi/2 > \varphi_1 > -\pi/2$ and $\pi/2 < \varphi_2 < 3\pi/2$. Already a slight misalignment of the propulsion directions for such angles leads to a rotation of the whole dumbbell until the squirmers' propulsion directions point (antiparallelly) apart from each other. The average bond force depends only very weakly on the active stress in the case $\beta_1 = |\beta_2|$ independent of Pe. This is consistent with the far-field prediction of the difference in the swimming velocities in the direction of the bond.[23,55] In as much as the propulsion directions are perfectly aligned, the active-stress contribution vanishes for $\beta_1 = |\beta_2|$ and the bond force is proportional to Pe. Deviations from a perfect parallel alignment imply small contributions of the active stress to the bond force, and $\langle F_b\rangle/Pe$ increases slightly with increasing Pe. Similarly, for ABP dumbbells, a linear increase in the bond force with increasing Pe is obtained, and dumbbell pairs of identical squirmers exhibit only a weak deviation from this dependence.[37] Our results are in contrast to predictions for athermal pusher–puller dumbbells with the same $|\beta_k|$,[23] where a parallel orientation of the propulsion directions, i.e., $\boldsymbol{e}_1 \cdot \boldsymbol{e}_2 = 1$, leads to stable swimming and a zero bond force. The differences in the forces emphasize the necessity to properly take into account thermal fluctuations. The latter are responsible for a particular relative alignment of the squirmers' propulsion directions, as discussed in Sec. V.

Noteworthy is the strong variation of the average bond force for pusher–puller combinations with $\beta_1 \neq |\beta_2|$. The results in Fig. 5 show that the force is the weakest for $\beta_1 = 1$ and $\beta_2 < -4$, and the strongest for $|\beta_k| = 3$. The strongest variations occur for combinations $\beta_1 - \beta_2 \approx 6$. As discussed in Sec. V, this is a consequence of a particular relative alignment of the propulsion directions. With the observed preferred alignments, the weak deviation of the bond force from the linear Pe dependence for the pairs $(\beta_1, \beta_2) = (1, -5)$ and $(\beta_1, \beta_2) = (1, -5)$ is consistent with the far-field prediction for the velocity difference,[23,55] especially due to the rather small variations in the alignment of the

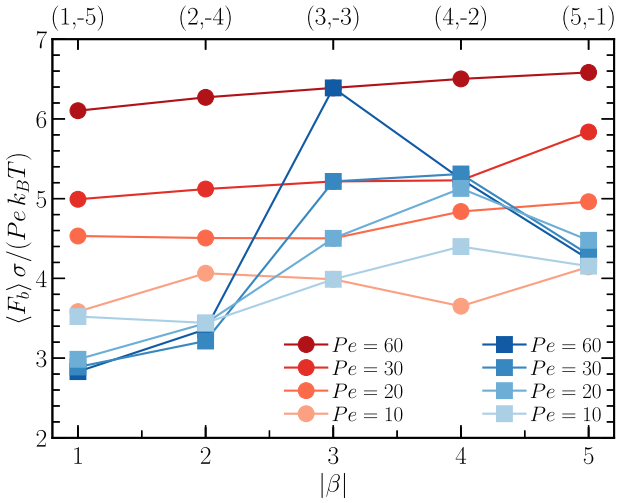

FIG. 5. Normalized average bond forces for various active-stress pairs (β_1, β_2) and Péclet numbers (see legend). The top-axis scale indicates various pairs (β_1, β_2) for the blue symbols. The red symbols are for pairs $\beta_1 = |\beta_2|$ (bottom axis).

propulsion directions with respect to the bond vector with increasing *Pe* (Sec. V B).

V. STATIONARY STATE SQUIRMER ORIENTATION

A. Relative alignment of propulsion directions

The interfering squirmer flow fields lead to preferred relative average orientations of the squirmers' propulsion directions. To quantify this preferred orientation, we consider the parameter

$$p = \langle \boldsymbol{e}_1 \cdot \boldsymbol{e}_2 \rangle = \langle \cos \vartheta \rangle, \tag{8}$$

which is the average of the cosine of the angle between the squirmers' propulsion directions.[37]

The dependence of p on the active stresses β_1 and β_2 is displayed in Fig. 6(a) in the form of a contour plot. Combinations of pusher–puller pairs with $\beta_1 = |\beta_2|$ exhibit only small variations with increasing magnitude β_1. This is emphasized in Fig. 7. In addition, Fig. 7 shows that $-1 < p < 0$ in this case, and hence, the relative orientation angle is in the range $180^\circ > \vartheta > 90^\circ$ for $60 \geq Pe \geq 10$. Thus, the squirmers' propulsion directions change from a nearly orthogonal orientation with respect to each other at small *Pe* to a nearly antiparallel orientation at large *Pe*. This can be understood in terms of the squirmers' vorticity flow field, which implies a preferred relative orientation of the propulsion directions.[23,55] In the limit $v_0 \to 0$, i.e., only the active stresses contribute to the flow field, the far-field approximation yields the stationary-state fixed point $\vartheta = 90^\circ$, i.e., an orthogonal orientation of the two propulsion directions for $\beta_1 = |\beta_2|$. In addition, a fixed point with $\varphi_1 = 180^\circ$ and $\varphi_2 = 0$ is obtained, corresponding to an antiparallel alignment of $\boldsymbol{e}_1$ and $\boldsymbol{e}_2$. Both fixed points are independent of $\beta_1 = |\beta_2|$. The thermal fluctuations strongly affect the stability of the fixed points and lead to relative alignments different from the predicted values (Fig. 7).

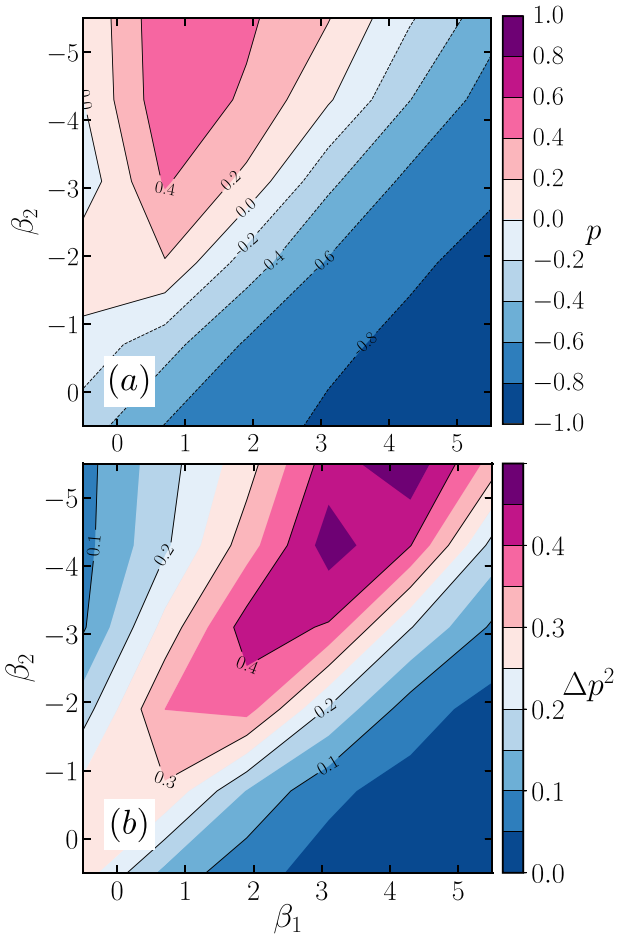

FIG. 6. (a) Average relative alignment of the squirmers' propulsion directions $p = \langle \boldsymbol{e}_1 \cdot \boldsymbol{e}_2 \rangle$ and (b) the variance Δp^2 as a function of their active stresses β_1 and β_2 for $Pe = 30$.

This explains the gradual shift of p from $p \approx 0$ to $p \approx -0.8$ with increasing *Pe*. Moreover, with increasing $Pe \gg 1$, the vorticity by the squirmer flow field becomes less relevant, and the relative orientation is determined only by the propulsion, with the fixed point $(\varphi_1, \varphi_2) = (180^\circ, 0)$.[23,55]

A different behavior is obtained for $\beta_1 \neq |\beta_2|$, with strong variations in the relative orientation, especially along the line $\beta_1 - \beta_2 \approx 6$ [Fig. 6(a)]. At $Pe = 30$, $p \approx 0.5$ for $(\beta_1, \beta_2) = (1, -5)$, and the angle $\vartheta \approx 60^\circ$ is the smallest compared to that of other pairs (β_1, β_2). The value $p \approx -0.8$ for various active-stress pairs, specifically for $(\beta_1, \beta_2) = (5, -1)$, is consistent with the fixed point $(\varphi_1, \varphi_2) = (180^\circ, 0)$ obtained from the vorticity.[23,55] Thermal fluctuations cause deviations from the predicted perfect antiparallel alignment, especially for smaller values of *Pe*. The alignment in the opposite limit $(\beta_1, \beta_2) = (1, -5)$ cannot simply be explained within the hydrodynamic far-field approximation for the vorticity. Here, the near-field effects or the coupling between the vorticity field by the active stresses and the swimming of the squirmers could be

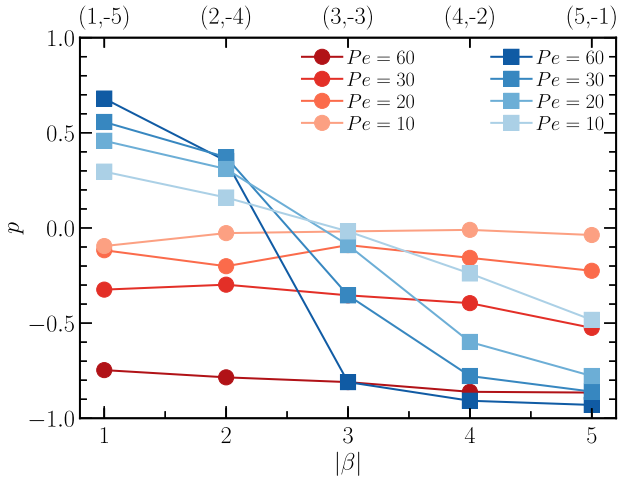

FIG. 7. Average relative alignment of the squirmers' propulsion directions $p = \langle \boldsymbol{e}_1 \cdot \boldsymbol{e}_2 \rangle$ as a function of the active-stress pairs $\beta_1 = |\beta_2|$ (bottom axis) and $\beta_1 \neq |\beta_2|$ (top axis), and various Péclet numbers *Pe*.

relevant. Evidently, the two combinations of active-stress magnitudes are not equivalent and lead to different swimming behaviors. This emphasizes the strong influence of the microswimmer flow field, specifically the strong impact of the bond, because the geometrical constraint by the bond is the causative for a particular orientation of the individual squirmers.

The dispersion of the relative orientation is quantified by the variance of p,

$$\Delta p^2 = \left\langle (\boldsymbol{e}_1 \cdot \boldsymbol{e}_2)^2 \right\rangle - p^2. \tag{9}$$

As displayed in Fig. 6(b), Δp^2 changes only weakly with the active stress in the case $\beta_1 = |\beta_2|$, but the variance is pronounced. The most severe fluctuations appear for the combinations $\beta_1 - \beta_2 \approx 6$. In particular, for $(\beta_1, \beta_2) \approx (3, -4)$, $|p|$ is rather small, and the relative alignment is weak, i.e., the hydrodynamic flow fields play a minor role in the orientational dynamics of the squirmers compared to the pronounced thermal fluctuations. Combinations with $(\beta_2, \beta_1) \approx (-5, 1)$ and $(\beta_2, \beta_1) \approx (-1, 5)$ exhibit rather weak fluctuations, which implies a quite stable alignment.

B. Alignment of propulsion direction with bond

The preferred orientation of the squirmers with respect to the bond vector is characterized by the parameters,

$$q_k = \langle \cos \varphi_k \rangle = \left\langle \frac{\boldsymbol{e}_k \cdot \boldsymbol{R}}{|\boldsymbol{R}|} \right\rangle. \tag{10}$$

The two squirmers show distinctively different q_k values as displayed in Fig. 8. The puller exhibits a wide range of orientations, with angles varying from $\varphi_1 \approx 75^\circ$ for $(\beta_1, \beta_2) = (1, -5)$ to $\varphi_1 \approx 150^\circ$ for $(\beta_1, \beta_2) = (5, -1)$, which is more clearly displayed in Fig. 9. The pusher [Fig. 8(b)] is preferentially aligned parallel to $\boldsymbol{R}$ with "average" angles in the range of $0 < \varphi_2 \lesssim 45^\circ$ and,

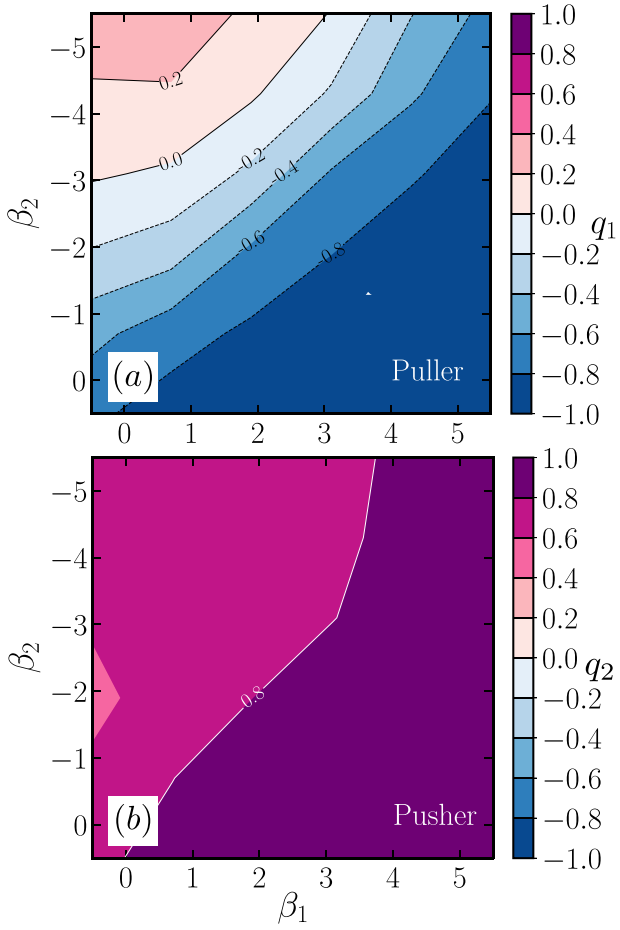

FIG. 8. Average alignment q_k of the squirmers' propulsion directions with respect to the bond vector as a function of their active stresses β_1 and β_2 at $Pe = 30$ for (a) the puller (q_1) and (b) the pusher (q_2).

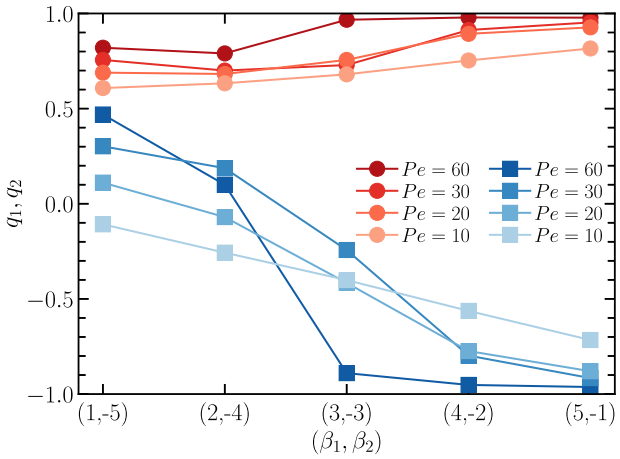

FIG. 9. Average alignment parameter q_k of the squirmers' propulsion direction $\boldsymbol{e}_k$ with the bond vector [Eq. (10)] as a function of the active-stress pairs $\beta_1 \neq |\beta_2|$ and various Péclet numbers. The blue symbols correspond to q_1 (puller) and the red ones correspond to q_2 (pusher).

hence, points always away from the puller for all combinations of β_1 and β_2. Figure 9 indicates an increasing preference in the alignment along the bond vector for both squirmers with increasing *Pe*, where the pusher is strongly aligned for all puller–pusher pairs, and the puller for pairs with $\beta_1 \geq 3$. Importantly, in these cases, the propulsion directions point in opposite directions away from each other.

As discussed in Sec. V A, the strong alignment of both squirmers for pairs with $\beta_1 \geq 3$, and especially large *Pe*, agrees with the theoretical prediction based on the far-field expression of the vorticity.[23,55] However, the large q_1 values for $\beta_1 < 3$ cannot simply be explained by vorticity, when the propulsion directions are located in the same plane as the bond vector. Here, the near-field effects may affect the relative alignment. The q_k values in Fig. 9 and the p_k values in Fig. 7 indicate that the two propulsion directions are, in general, twisted with respect to a plane including the bond vector. By characterizing the twist using the quantity $\cos\chi = (\boldsymbol{e}_1 \times \boldsymbol{R}/|\boldsymbol{R}|) \cdot \boldsymbol{e}_2$, where χ is the torsional angle, we find nearly zero averages for $\cos\chi$, reflecting the symmetry in the orientations of $\boldsymbol{e}_1$ and $\boldsymbol{e}_2$ with respect the torsional plane. However, the average $\langle|\cos\chi|\rangle$ is non-zero, and we find $\langle|\cos\chi|\rangle \approx 0.2$, which suggests an out-of-plane twist induced by the flow. This twist may be responsible for the observed preference in the alignment of the $\boldsymbol{e}_k$ with respect to the bond vector, specifically for $\beta_1 < 3$.

VI. DUMBBELL DYNAMICS

Figure 10 displays examples of dumbbell center-of-mass trajectories for various active-stress pairs. The trajectories of pairs with $\beta_1 = |\beta_2|$ are rather similar. Stronger variations in the dynamics appear for the pairs $(\beta_1,\beta_2) = (1,-5)$ and $(\beta_1,\beta_2) = (5,-1)$, with a smaller displacement for the latter.

This difference is reflected in the center-of-mass mean-square displacement (MSD) in Fig. 11. For every puller–pusher pair, we find a close-to-ballistic short-time dynamics, which turns into a long-time diffusive motion. The crossover between the two regimes is determined by the effective rotational diffusion coefficient, which

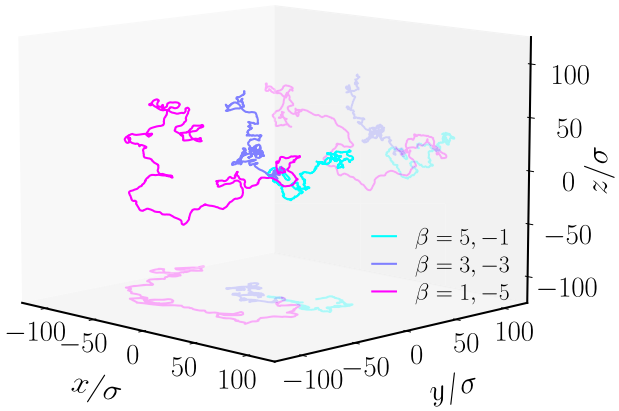

FIG. 10. Dumbbell center-of-mass trajectories for the active-stress pairs $(\beta_1,\beta_2) = (5,-1), (3,-3), (1,-5)$ at $Pe = 30$ with the respective projections onto the xy and xz planes.

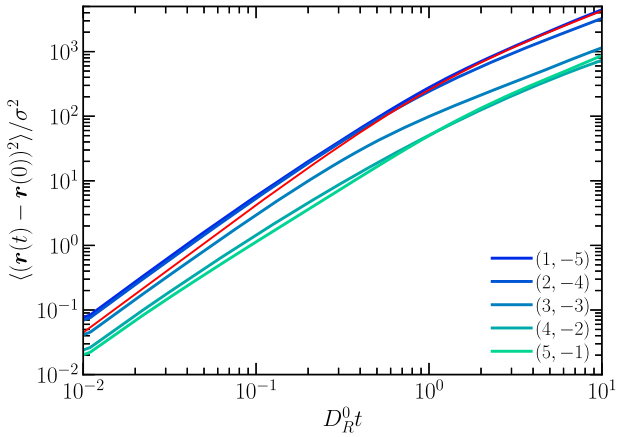

FIG. 11. Dumbbell center-of-mass mean-square displacement as a function of the scaled time $D_R^0 t$ for the indicated active-stress pairs, and the Péclet number $Pe = 30$. The red line indicates the corresponding ABP dumbbell theoretical prediction [Eq. (11)].

depends on *Pe* and the active-stress combination [cf. Fig. 3(b)]. The change from a weak puller–strong pusher $(\beta_1,\beta_2) = (1,-5)$ pair to a strong pusher–weak puller $(\beta_1,\beta_2) = (5,-1)$ pair slows down the MSD considerably. The comparison of the squirmer dumbbell MSD with the active MSD contribution of an ABP dumbbell,[37,46,56]

$$\left\langle (\boldsymbol{r}(t) - \boldsymbol{r}(0))^2 \right\rangle = \frac{v_0^2}{\gamma_R^2}\left(\gamma_R t + e^{-\gamma_R t} - 1\right), \tag{11}$$

yields good agreement at long times for the pair $(\beta_1,\beta_2) = (1,-5)$. In the active ballistic regime, the swimming velocity is affected by the squirmer flow fields for all active-stress combinations, but the active diffusive motion is quantitatively captured by the theoretical expression.

Figure 12 presents active translational diffusion coefficients D_T for various active-stress pairs extracted from the linear long-time regime of the MSD. Except for the pair $(\beta_1,\beta_2) = (1,-5)$ at $Pe = 60$, the D_T values are smaller than the value of D_T^0 for an ABP dumbbell. Interestingly, D_T is, within the accuracy of the simulations, independent of β for pairs with $\beta_1 = |\beta_2|$. Merely the values for $Pe = 60$ increase with increasing β_k. In terms of *Pe*-dependence, the diffusion coefficient decreases significantly with increasing *Pe*. At $Pe = 60$ and $\beta = 1$, D_T is about a factor of 20 smaller than D_T^0. We expect D_T to further decrease with increasing *Pe*. For the considered mixed pairs, the dependence on *Pe* is weaker as long as $\beta_1 \neq |\beta_2|$. In particular, the ratio D_T/D_T^0 seems to approach an *Pe*-independent value for $(\beta_1,\beta_2) = (5,-1)$. The decrease of D_T with increasing *Pe*, especially for pairs with $\beta_1 > 3$ and $\beta_2 > -3$, is related to the antiparallel alignment of the propulsion directions as well as their twist. However, D_T is still activity dependent and increases with increasing *Pe*, since $D_T^0 \sim Pe^2$.

The variation of the diffusion coefficient with the active stress of puller–pusher pairs is orders of magnitude smaller than that of dumbbells comprising identical squirmers.[37] This is related to the stronger orientational preference of the latter, specifically a

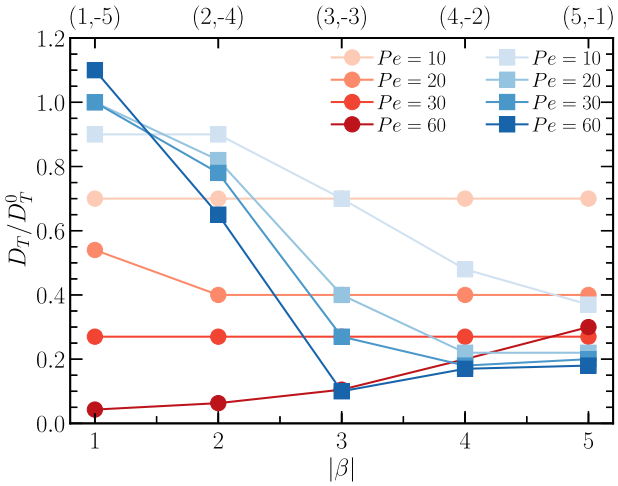

FIG. 12. Active diffusion coefficients, D_T, obtained from the long-time linear time regime of the MSD for the indicated active-stress pairs and Péclet numbers. $D_T^0 = Pe^2 D_R^0 \sigma^2/12$ is the diffusion coefficient of the ABP dumbbell [Eq. (11)].

strong antiparallel alignment of the propulsion directions of pullers with large active stress, and correspondingly a very small diffusion coefficient.

The simulations of Ref. 18 suggest that any quantity of a 1:1 mixture of (independent) pushers and pullers, which depends on the spatial and temporal velocity correlation function, coincides with that of a suspension of noninteracting swimmers. This approximately applies to the MSD of our dumbbells at short times for $\beta_1 = |\beta_2|$ when compared with the MSD of ABP dumbbells, but not for longer times and pusher–puller pairs with large differences in the magnitude of the active stress. Evidently, the presence of a bond plays an important role in addition to the asymmetry of the squirmer flow fields.

VII. SUMMARY AND CONCLUSIONS

We have performed mesoscale hydrodynamic simulations of active squirmer dumbbells composed of pusher and puller monomers by applying the multiparticle collision dynamics approach for the fluid. By varying the magnitudes $|\beta_k|$ of their active stress, we have analyzed the emerging conformational and dynamical properties of the asymmetric squirmer dumbbells.

The distinct squirmer flow fields and the geometric constraint by the bond promote a specific, active-stress-dependent rotational dynamics of the individual squirmers as well as the dumbbell itself, a preferred average relative orientation of their propulsion directions, and an active diffusional motion. In the case of equal active-stress magnitudes, $\beta_1 = |\beta_2|$, orientations and dynamical quantities typically depend only weakly on the stress magnitude. However, the variation with the Péclet number can be large. Pronounced changes in the emergent properties appear for asymmetric pairs with strongly differing active stresses, especially for the pairs $(\beta_1, \beta_2) = (1, -5)$ and $(\beta_1, \beta_2) = (5, -1)$. Here, the interference of the squirmers' flow fields strongly influences the orientational properties of the puller with respect to the bond vector, whereas the orientation $\boldsymbol{e}_2$ of the pusher is nearly unaffected. This governs ultimately the dumbbells' translational motion.

The analytical studies of Ref. 23, based on athermal squirmer dumbbells, predict a zero bond force for all pusher–puller pairs with parallelly aligned propulsion directions along the bond vector and the same $|\beta_k|$. In our simulations, the average bond force is always non-zero due to the thermal fluctuations in the squirmers' propulsion directions, and the configuration with parallel $\boldsymbol{e}_k$ is unstable. This emphasizes the role of thermal fluctuations on microswimmers (microbots) and their emergent properties.

Neither the weak dependence of the active translation diffusion coefficient D_T on $|\beta_k|$ of dumbbells with $\beta_1 = |\beta_2|$ nor the good agreement of the MSD of the dumbbell for $(\beta_1, \beta_2) = (1, -5)$ with the theoretical expression of the MSD of an ABP dumbbell indicates a cancellation of hydrodynamic correlations as is observed in 1:1 pusher–puller mixtures.[18] In contrast, in all considered cases, the hydrodynamic correlation plays a major role, which is reflected in the strong orientational correlations of the squirmers and the dependence of D_T on the Péclet number.

We have focused on the separation $l/\sigma = 4/3$ of the two squirmers, which yields significant near-field hydrodynamic interactions between the squirmers. The studies provide, in combination with thermal fluctuations, deeper insight into the properties of microscale active assemblies, reaching beyond the far-field predictions of athermal dumbbells.[23] Our studies on the distance dependence of the relative alignment of the propulsion directions for squirmer dumbbells with $\beta_1 = \beta_2$ reveal a decreasing influence of the flow field with increasing distance, as expected from the spatial decay of hydrodynamic interactions. Qualitatively, a similar reduction is expected of the considered systems with $\beta_1 \neq \beta_2$.

Our simulations indicate that the properties of microbots can be controlled by suitable combinations of pusher–puller pairs. An asymmetric combination with a strong pusher and a weak puller slightly enhances the swimming performance compared to an ABP dumbbell at large Pe and reduces bond stress, whereas an opposite combination leads to a considerable slowing down of the active diffusive motion. In fact, the MSD of an active ABP dumbbell is only half of that of an individual ABP or squirmer. Thus, a combination of squirmers typically leads to a slowdown of their dynamics compared to an individual squirmer. Nevertheless, by dynamically changing the active stresses of squirmers in a dumbbell, the translational motion can be tuned. In contrast, the properties of pairs of squirmers with the same $|\beta_k|$ are less sensitive to changes in the magnitude of the active stress, and hence, they are also less sensitive to possible polydispersity effects.

SUPPLEMENTARY MATERIAL

The supplementary material provides movies, which illustrate the alignment of the propulsion directions of the individual squirmers, their individual rotational diffusive motion, and the rotational diffusive dynamics of a dumbbell itself in the dumbbell center-of-mass reference frame. Movies for the active-stress pairs $(\beta_1, \beta_2) = (1, -5)$ (M1), $(\beta_1, \beta_2) = (3, -3)$ (M2), and $(\beta_1, \beta_2) = (5, -1)$ (M3) are shown. The Péclet number is $Pe = 30$. The squirmer with the blue semisphere is the pusher, and the one with the red semisphere is the puller.

AUTHOR DECLARATIONS

Conflict of Interest

The authors have no conflicts to disclose.

DATA AVAILABILITY

The data that support the findings of this study are available from the corresponding authors upon reasonable request.

REFERENCES

[1] T. Kiørboe, H. Jiang, R. J. Gonçalves, L. T. Nielsen, and N. Wadhwa, Proc. Natl. Acad. Sci. U. S. A. **111**, 11738 (2014).
[2] I. Tuval, L. Cisneros, C. Dombrowski, C. W. Wolgemuth, J. O. Kessler, and R. E. Goldstein, Proc. Natl. Acad. Sci. U. S. A. **102**, 2277 (2005).
[3] K. Drescher, K. C. Leptos, I. Tuval, T. Ishikawa, T. J. Pedley, and R. E. Goldstein, Phys. Rev. Lett. **102**, 168101 (2009).
[4] S. E. Spagnolie and E. Lauga, J. Fluid Mech. **700**, 105 (2012).
[5] M. Theers, E. Westphal, G. Gompper, and R. G. Winkler, Soft Matter **12**, 7372 (2016).
[6] J. Hu, A. Wysocki, R. G. Winkler, and G. Gompper, Sci. Rep. **5**, 9586 (2015).
[7] S. Bianchi, F. Saglimbeni, and R. Di Leonardo, Phys. Rev. X **7**, 011010 (2017).
[8] S. M. Mousavi, G. Gompper, and R. G. Winkler, Soft Matter **16**, 4866 (2020).
[9] K. Drescher, R. E. Goldstein, N. Michel, M. Polin, and I. Tuval, Phys. Rev. Lett. **105**, 168101 (2010).
[10] K. Drescher, J. Dunkel, L. H. Cisneros, S. Ganguly, and R. E. Goldstein, Proc. Natl. Acad. Sci. U. S. A. **108**, 10940 (2011).
[11] J. Hu, M. Yang, G. Gompper, and R. G. Winkler, Soft Matter **11**, 7867 (2015).
[12] T. Ishikawa, J. R. Soc. Interface **6**, 815 (2009).
[13] E. Lauga and T. R. Powers, Rep. Prog. Phys. **72**, 096601 (2009).
[14] J. Elgeti, R. G. Winkler, and G. Gompper, Rep. Prog. Phys. **78**, 056601 (2015).
[15] O. S. Pak and E. Lauga, J. Eng. Math. **88**, 1 (2014).
[16] K. Qi, H. Annepu, G. Gompper, and R. G. Winkler, Phys. Rev. Res. **2**, 033275 (2020).
[17] A. V. Singh, V. Kishore, G. Santomauro, O. Yasa, J. Bill, and M. Sitti, Langmuir **36**, 5435–5443 (2020).
[18] D. Bárdfalvy, S. Anjum, C. Nardini, A. Morozov, and J. Stenhammar, Phys. Rev. Lett. **125**, 018003 (2020).
[19] G. Pessot, H. Löwen, and A. M. Menzel, Mol. Phys. **116**, 3401 (2018).
[20] C. Bechinger, R. Di Leonardo, H. Löwen, C. Reichhardt, G. Volpe, and G. Volpe, Rev. Mod. Phys. **88**, 045006 (2016).
[21] H. Ceylan, J. Giltinan, K. Kozielski, and M. Sitti, Lab Chip **17**, 1705 (2017).
[22] S. Palagi and P. Fischer, Nat. Rev. Mater. **3**, 113 (2018).
[23] T. Ishikawa, Micromachines **10**, 33 (2019).
[24] G. Gompper, R. G. Winkler, T. Speck, A. Solon, C. Nardini, F. Peruani, H. Löwen, R. Golestanian, U. B. Kaupp, L. Alvarez, T. Kiørboe, E. Lauga, W. C. K. Poon, A. DeSimone, S. Muiños-Landin, A. Fischer, N. A. Söker, F. Cichos, R. Kapral, P. Gaspard, M. Ripoll, F. Sagues, A. Doostmohammadi, J. M. Yeomans, I. S. Aranson, C. Bechinger, H. Stark, C. K. Hemelrijk, F. J. Nedelec, T. Sarkar, T. Aryaksama, M. Lacroix, G. Duclos, V. Yashunsky, P. Silberzan, M. Arroyo, and S. Kale, J. Phys.: Condens. Matter **32**, 193001 (2020).
[25] R. G. Winkler and G. Gompper, J. Chem. Phys. **153**, 040901 (2020).
[26] H. R. Vutukuri, M. Lisicki, E. Lauga, and J. Vermant, Nat. Commun. **11**, 2628 (2020).
[27] A. C. H. Tsang, E. Demir, Y. Ding, and O. S. Pak, Adv. Intell. Syst. **2**, 1900137 (2020).
[28] T.-Y. Huang, H. Gu, and B. J. Nelson, Annu. Rev. Control Robot. Auton. Syst. **5**, 279 (2022).
[29] R. W. Carlsen and M. Sitti, Small **10**, 3831 (2014).
[30] M. J. Lighthill, Commun. Pure Appl. Math. **5**, 109 (1952).
[31] J. R. Blake, J. Fluid Mech. **46**, 199 (1971).
[32] T. Ishikawa, M. P. Simmonds, and T. J. Pedley, J. Fluid Mech. **568**, 119 (2006).
[33] A. Zöttl and H. Stark, Eur. Phys. J. E **41**, 61 (2018).
[34] F. J. Schwarzendahl and M. G. Mazza, J. Chem. Phys. **150**, 184902 (2019).
[35] D. Bárdfalvy, H. Nordanger, C. Nardini, A. Morozov, and J. Stenhammar, Soft Matter **15**, 7747 (2019).
[36] M. Wagner, S. Roca-Bonet, and M. Ripoll, Eur. Phys. J. E **44**, 43 (2021).
[37] J. Clopés, G. Gompper, and R. G. Winkler, Soft Matter **16**, 10676 (2020).
[38] R. Kapral, Adv. Chem. Phys. **140**, 89 (2008).
[39] G. Gompper, T. Ihle, D. M. Kroll, and R. G. Winkler, "Multi-particle collision dynamics: A particle-based mesoscale simulation approach to the hydrodynamics of complex fluids," Adv. Polym. Sci. **221**, 1 (2009).
[40] I. O. Götze and G. Gompper, Phys. Rev. E **82**, 041921 (2010).
[41] M. Theers, E. Westphal, K. Qi, R. G. Winkler, and G. Gompper, Soft Matter **14**, 8590 (2018).
[42] Y.-G. Tao and R. Kapral, J. Chem. Phys. **128**, 164518 (2008).
[43] M. T. Downton and H. Stark, J. Phys.: Condens. Matter **21**, 204101 (2009).
[44] A. Zöttl and H. Stark, Phys. Rev. Lett. **112**, 118101 (2014).
[45] K. Qi, E. Westphal, G. Gompper, and R. G. Winkler, Phys. Rev. Lett. **124**, 068001 (2020).
[46] R. G. Winkler, Soft Matter **12**, 3737 (2016).
[47] H. Noguchi and G. Gompper, Phys. Rev. E **78**, 016706 (2008).
[48] M. Theers and R. G. Winkler, Phys. Rev. E **91**, 033309 (2015).
[49] C.-C. Huang, A. Chatterjii, G. Sutmann, G. Gompper, and R. G. Winkler, J. Comput. Phys. **229**, 168 (2010).
[50] T. Ihle and D. M. Kroll, Phys. Rev. E **67**, 066705 (2003).
[51] E. Westphal, S. P. Singh, C.-C. Huang, G. Gompper, and R. G. Winkler, Comput. Phys. Commun. **185**, 495 (2014).
[52] I. P. Omelyan, Phys. Rev. E **58**, 1169 (1998).
[53] A. Lamura, G. Gompper, T. Ihle, and D. M. Kroll, Europhys. Lett. **56**, 319 (2001).
[54] M. Kuron, P. Stärk, C. Burkard, J. de Graaf, and C. Holm, J. Chem. Phys. **150**, 144110 (2019).
[55] I. Llopis and I. Pagonabarraga, J. Non-Newtonian Fluid Mech. **165**, 946 (2010).
[56] Equation (10) of Ref. 28 contains an error. The factor 2 in front of v_0^2 should be replaced by unity.